Supporting information

High-entropy-alloy Nanoparticles Synthesized by Laser Metallurgy using Multivariate MOF

Wei Yan,‡[ad] Haoqing Jiang,‡[bc] Wendi Yi,‡[c] Chengbin Zhao,[d] Yucong Xia,[d] Hengjiang Cong,[d] Lin Tang,*[ab] Gary J. Cheng,*[ce] Jianhua He,*[a] and Hexiang Deng*[abd]

[a] *The Institute for Advanced Studies*, *Wuhan University*, *Wuhan 430072*, *China*

[b] *Hubei Yangtze Memory Laboratories*, *Wuhan 430205*, *China*

[c] *The Institute of Technological Sciences*, *Wuhan University*, *Wuhan 430072*, *China*

[d] *College of Chemistry and Molecular Sciences*, *Wuhan University*, *Wuhan 430072*, *China*

[e] *School of Industrial Engineering*, *Purdue University*, *West Lafayette 47906*, *IN*, *USA*

‡ These authors contributed equally to this work

Table of Contents

Section S1. Synthesis of organic linkers

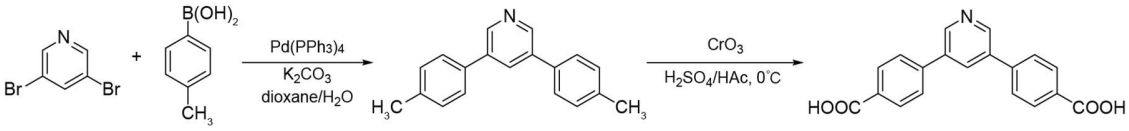

Fig. S1. General scheme for the synthesis of 3,5-di-*p*-tolylpyridine (DPT) and 4,4'-(pyridine-3,5-diyl)dibenzoic acid (PDA)

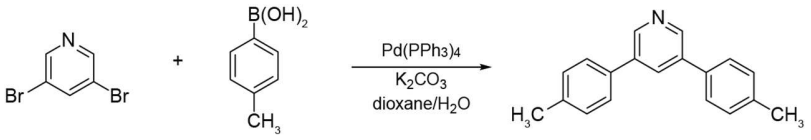

Fig. S2. Scheme for the synthesis of DPT

3,5-dibromopyridine (4.74g, 20 mmol), *p*-tolylboronic acid (8.16g, 60 mmol), potassium carbonate (8.29 g, 60 mmol) and $Pd(PPh_3)_4$ (1.16g, 1 mmol) were added to a Schlenk flask. The flask was then capped with a rubber septum, evacuated and backfilled with argon three times. Under an inert atmosphere, degassed 1,4-dioxane (125 mL) and H_2O (25 mL) were added via syringe. Then, the mixture was heated in 110 °C for 3 days. After that, the crude product was extracted with EtOAc (3 × 150 mL), the combined organic phases were washed with brine (300 mL), dried over Na_2SO_4 and concentrated in vacuo. Pure product was obtained from column chromatography using PE / EtOAc as the eluent. The desired product DPT was obtained as a faint yellow solid (4.51 g, 17.4 mmol, 87%) (S1).

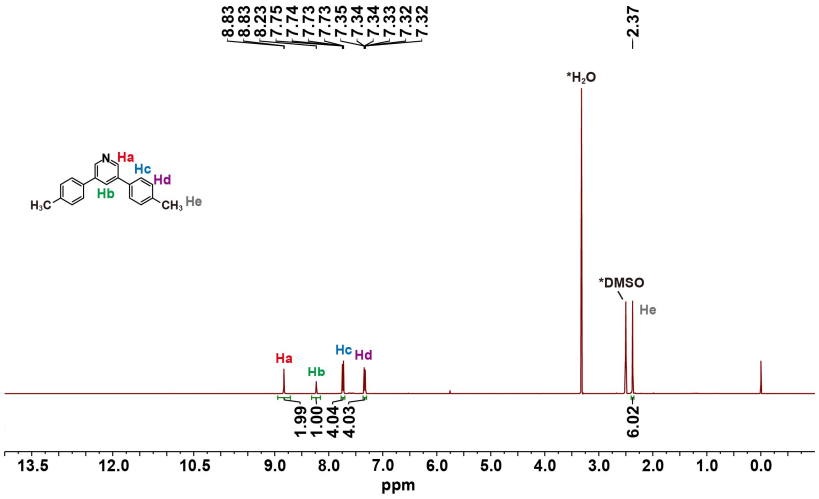

Fig. S3 ^{1}H NMR spectrum of compound DPT

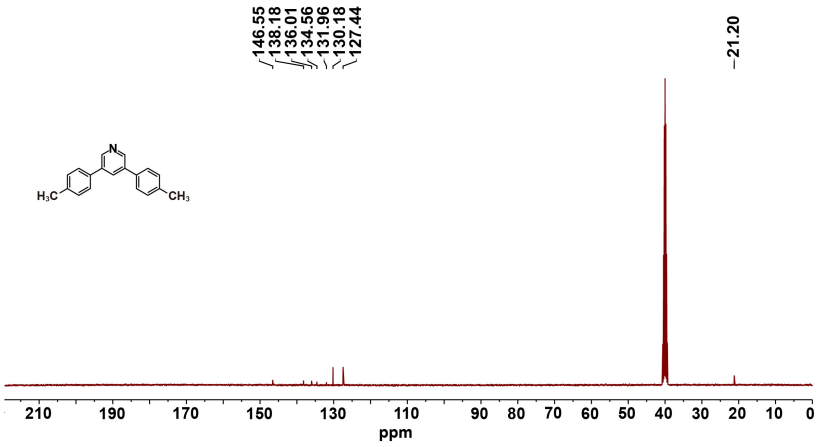

Fig. S4 ^{13}C NMR spectrum of compound DPT

Synthesis of 4,4'-(pyridine-3,5-diyl)dibenzoic acid (PDA)

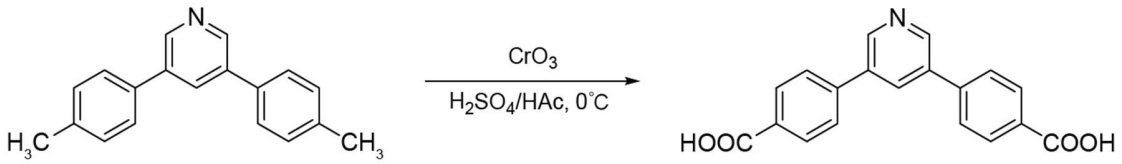

Fig. S5. Scheme for the synthesis of PDA

CrO_3 (5.94 g, 59.4 mmol) was added to a solution of conc sulfuric acid (0.2 ml), glacial acetic acid (35 ml) and acetic anhydride (1.5 ml, 16 mmol) cooled at 20 °C in a water-ice bath. DPT (1.27 g, 4.9 mmol) was added in small portions with stirring, while the reaction temperature was kept below 35 °C using the ice-water bath. After the addition was complete, the reaction was heated to 120 °C and stirred at this temperature for 4 h. The mixture was then cooled to room temperature and poured into water (400 mL), and the resulting precipitate collected by filtration. The white solid was washed with water and air-dried to give 4,4'-(pyridine-3,5-diyl)dibenzoic acid (PDA) as a white solid (1.53 g, 98%) (S2).

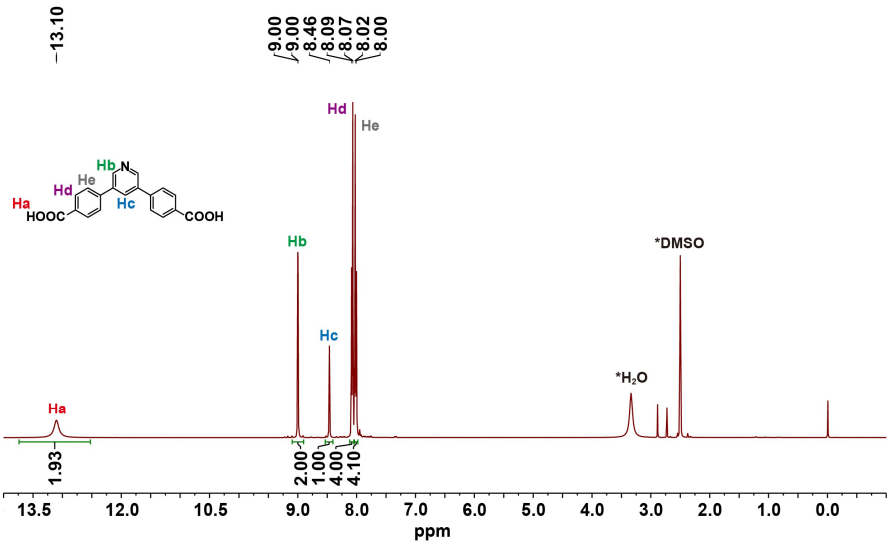

Fig. S6 ^{1}H NMR spectrum of compound PDA

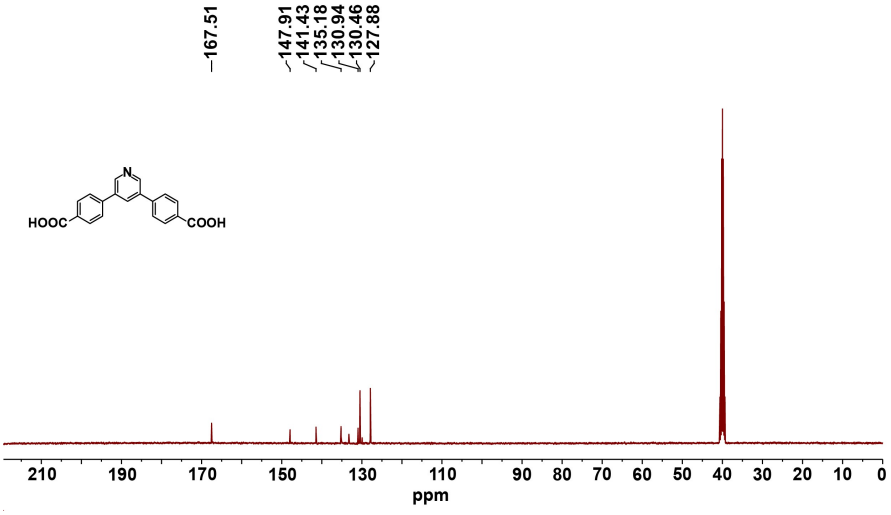

Fig. S7 ^{13}C NMR spectrum of compound PDA

Section S2. Synthesis and activation of MOFs

The crystallinity and purity of these MOFs were confirmed by powder X-ray diffraction (PXRD) and single crystal X-ray diffraction (SC-XRD) techniques. PXRD patterns were measured on a Rigaku Smartlab 9KW diffractometer operated at 45 kV, 200 mA using Cu Kα (λ = 1.5406 Å) with a scanning speed of 5°/min, and a step of 0.01° in 2θ at ambient temperature and pressure. Simulated PXRD patterns were calculated using software Material Studio 8.0 using the corresponding single crystal data.

The fresh MOF samples must be activated prior to any gas sorption measurements. Firstly, the samples were treated with solvent exchange with DMF for 3 days at room temperature and exchanged three times each day. After that, these samples were immersed in acetone for another 3 days at room temperature and exchanged three times each day. Secondly, the remaining acetone in the MOF samples was removed by supercritical CO_2. For this step, the acetone-containing sample was placed in the chamber and the solvent was completely exchanged with liquid CO_2. After this exchange, the chamber was heated up to 40 °C and held on at the supercritical condition (typically 1300 psi) for 45 min. The CO_2 was slowly vented (ca. 8 h) from the chamber at around 38 °C, thus generating the solvent-free porous MOF samples. After the activation, N_2 adsorption isotherms of these MOFs were measured to confirm the permanent porosity. PXRD of the activated MOF samples matched well with the simulated pattern based on single crystal structure.

Optical microscope images of single crystal of MOFs

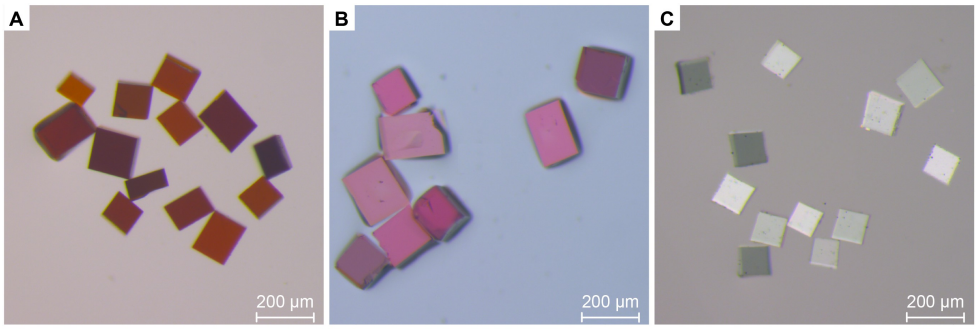

Fig. S8 Optical microscope images of (A) CPM-70-Fe; (B) CPM-70-Co; (C) CPM-70-Ni

Synthesis of MOFs and PXRD pattern

Synthesis and activation of CPM-70-Fe

$Fe(NO_3)_3 \cdot 9H_2O$ (20 mg), PDA (12 mg), trifluoroacetate (120 μL) in 2 mL of DMF were ultrasonically dissolved in a 4 mL Pyrex vial. The mixture was heated in a 150 °C

oven for 24 h. After cooling down to room temperature, dark brown cubic crystals were yielded (Fig. S8).

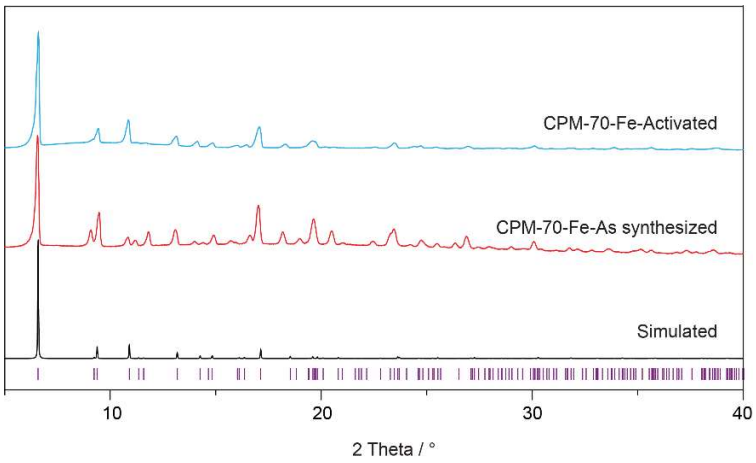

Fig. S9 Comparison of the experimental PXRD pattern of as-synthesized and activated CPM-70-Fe with the simulated CPM-70-Fe diffraction pattern based on its single crystal data.

Synthesis and activation of CPM-70-Co

$Co(NO_3)_2 \cdot 6H_2O$ (29 mg), PDA (32 mg), fluoboric acid (20 μL) in 4 mL of DMA were ultrasonically dissolved in a 20 mL Pyrex vial. The mixture was heated in a 130 °C oven for 72h. After cooling down to room temperature, red cubic crystals were yielded (Fig. S8).

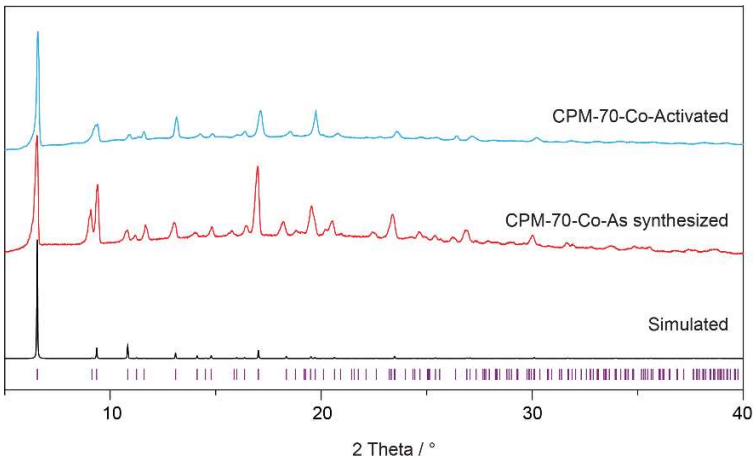

Fig. S10 Comparison of the experimental PXRD pattern of as-synthesized and activated CPM-70-Co with the simulated CPM-70-Co diffraction pattern based on its single crystal data.

Synthesis and activation of CPM-70-Ni

$Ni(NO_3)_2 \cdot 6H_2O$ (20 mg), PDA (10 mg), trifluoroacetate (100 μL) in 2.5 mL of DMF were ultrasonically dissolved in a 4 mL Pyrex vial. The mixture was heated in a 150 °C

oven for 24h. After cooling down to room temperature, faint green cubic crystals were yielded (Fig. S8).

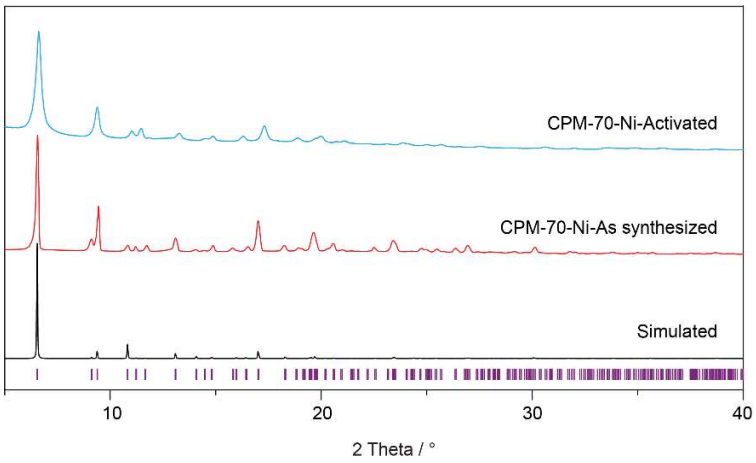

Fig. S11 Comparison of the experimental PXRD pattern of as-synthesized and activated CPM-70-Ni with the simulated CPM-70-Ni diffraction pattern based on its single crystal data.

Synthesis and activation of CPM-70-FeCo

$Fe(NO_3)_3 \cdot 9H_2O$ (10 mg), $Co(NO_3)_2 \cdot 6H_2O$ (7.2 mg), PDA (10 mg), trifluoroacetate (100 μL) in 2.5 mL of DMF were ultrasonically dissolved in a 4 mL Pyrex vial. The mixture was heated in a 150 °C oven for 24h. After cooling down to room temperature, brown powders were yielded.

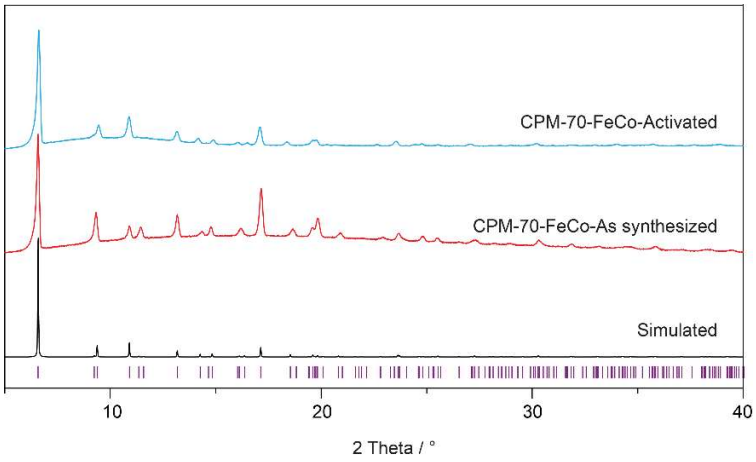

Fig. S12 Comparison of the experimental PXRD pattern of as-synthesized and activated CPM-70-FeCo with the simulated CPM-70-Fe diffraction pattern based on its single crystal data.

Synthesis and activation of CPM-70-FeNi

$Fe(NO_3)_3 \cdot 9H_2O$ (10 mg), $Ni(NO_3)_2 \cdot 6H_2O$ (7.2 mg), PDA (10 mg), trifluoroacetate

(100 μL) in 2.5 mL of DMF were ultrasonically dissolved in a 4 mL Pyrex vial. The mixture was heated in a 150 °C oven for 24h. After cooling down to room temperature, dark green powders were yielded.

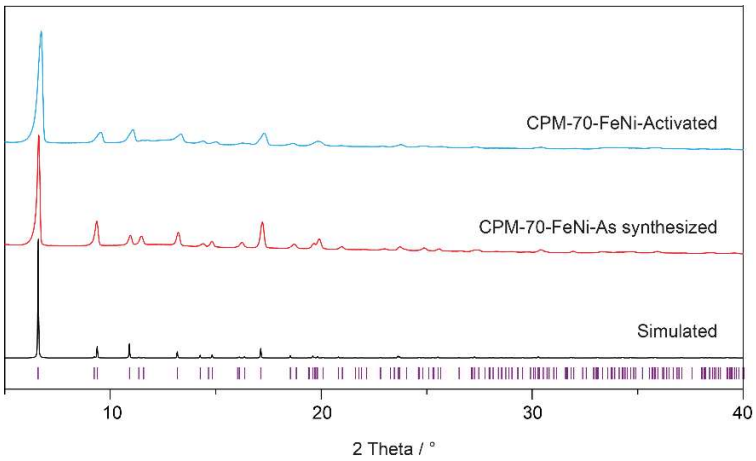

Fig. S13 Comparison of the experimental PXRD pattern of as-synthesized and activated CPM-70-FeNi with the simulated CPM-70-Fe diffraction pattern based on its single crystal data.

Synthesis and activation of CPM-70-FeCoNi

$Fe(NO_3)_3 \cdot 9H_2O$ (10 mg), $Co(NO_3)_2 \cdot 6H_2O$ (7.2 mg), $Ni(NO_3)_2 \cdot 6H_2O$ (7.2 mg), PDA (10 mg), trifluoroacetate (100 μL) in 2.5 mL of DMF were ultrasonically dissolved in a 4 mL Pyrex vial. The mixture was heated in a 150 °C oven for 24h. After cooling down to room temperature, brown powders were yielded.

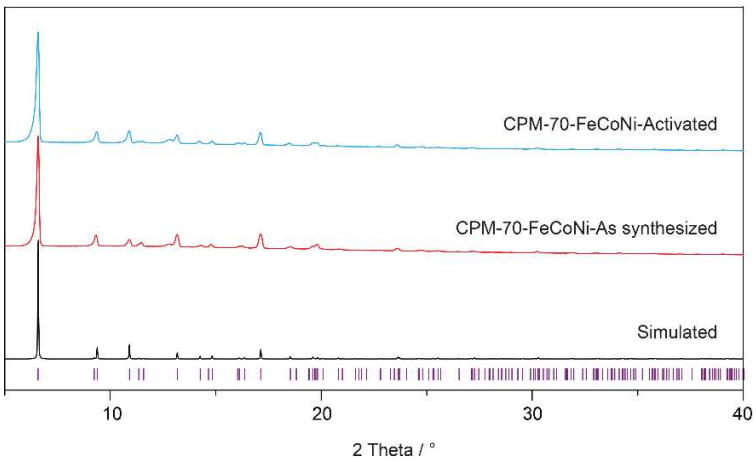

Fig. S14 Comparison of the experimental PXRD pattern of as-synthesized and activated CPM-70-FeCoNi with the simulated CPM-70-Fe diffraction pattern based on its single crystal data.

Synthesis and activation of CPM-70-MnFeCoNiCu

$Fe(NO_3)_3 \cdot 9H_2O$ (10 mg), $Co(NO_3)_2 \cdot 6H_2O$ (7.2 mg), $Ni(NO_3)_2 \cdot 6H_2O$ (7.2 mg), $Mn(NO_3)_2 \cdot 4H_2O$ (6.2 mg), $Cu(NO_3)_2 \cdot 3H_2O$ (6 mg), PDA (10 mg), trifluoroacetate (100 μL) in 2.5 mL of DMF were ultrasonically dissolved in a 4 mL Pyrex vial. The mixture was heated in a 150 °C oven for 24h. After cooling down to room temperature, brown powders were yielded.

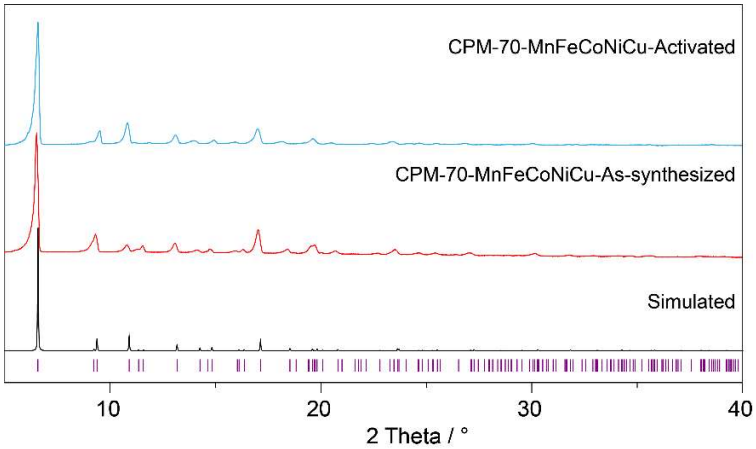

Fig. S15 Comparison of the experimental PXRD pattern of as-synthesized and activated CPM-70-Fe-Co-Ni with the simulated CPM-70-Fe diffraction pattern based on its single crystal data.

Synthesis and activation of CPM-70-MnFeCoNiZn

$Fe(NO_3)_3 \cdot 9H_2O$ (10 mg), $Co(NO_3)_2 \cdot 6H_2O$ (7.2 mg), $Ni(NO_3)_2 \cdot 6H_2O$ (7.2 mg), $Mn(NO_3)_2 \cdot 4H_2O$ (6.2 mg), $Zn(NO_3)_2 \cdot 6H_2O$ (7.3 mg), PDA (10 mg), trifluoroacetate (100 μL) in 2.5 mL of DMF were ultrasonically dissolved in a 4 mL Pyrex vial. The mixture was heated in a 150 °C oven for 24h. After cooling down to room temperature, brown powders were yielded.

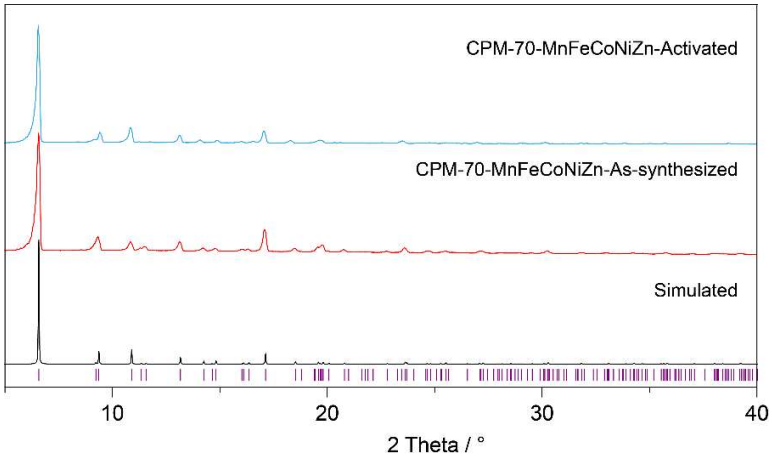

Fig. S16 Comparison of the experimental PXRD pattern of as-synthesized and activated CPM-70-FeCoNi with the simulated CPM-70-Fe diffraction pattern based on its single crystal data.

Table S1. Crystal data and structure refinement for CPM-70-Fe

Empirical formula	$C_{57}H_{33}Fe_3N_3O_{13}$
Formula weight	1135.41
Temperature/K	296.15
Crystal system	trigonal
Space group	*R*-3*c*
a /Å	19.3981(13)
b /Å	19.3981(13)
c /Å	45.548(3)
α /°	90
β /°	90
γ /°	120
Volume/Å^3	14843(2)
Z	6
ρ_{calc}g/cm^3	0.762
μ/mm^{-1}	3.784
F(000)	3468.0
Radiation	CuKα (λ = 1.54178)
2θ range for data collection/°	6.538 to 130.42
Index ranges	$-22 \leq h \leq 19$, $-22 \leq k \leq 18$, $-52 \leq l \leq 46$
Reflections collected	22609
Independent reflections	2810 [R_{int} = 0.0537, R_{sigma} = 0.0295]
Data/restraints/parameters	2810/0/118
Goodness-of-fit on F^2	1.071
Final R indexes [I>=2σ (I)]	R_1 = 0.0588, wR_2 = 0.1783
Final R indexes [all data]	R_1 = 0.0642, wR_2 = 0.1843
Largest diff. peak/hole / e Å^{-3}	0.84/-0.47

Table S2. Crystal data and structure refinement for CPM-70-Co

Empirical formula	$C_{57}H_{33}Co_3N_3O_{13}$
Formula weight	1144.65
Temperature/K	296.15
Crystal system	trigonal
Space group	*R*-3*c*
a /Å	19.3302(3)
b /Å	19.3302(3)
c /Å	45.7445(16)
α /°	90
β /°	90
γ /°	120
Volume/Å^3	14802.7(7)
Z	6
ρcalcg/cm^3	0.770
μ/mm^{-1}	4.208
F(000)	3486.0
Radiation	CuKα (λ = 1.54178)
2θ range for data collection/°	6.542 to 130.114
Index ranges	$-18 \leq h \leq 21$, $-22 \leq k \leq 18$, $-46 \leq l \leq 53$
Reflections collected	25587
Independent reflections	2816 [Rint = 0.0633, Rsigma = 0.0371]
Data/restraints/parameters	2816/18/117
Goodness-of-fit on F^2	1.072
Final R indexes [I>=2σ (I)]	R1 = 0.0787, wR2 = 0.2310
Final R indexes [all data]	R1 = 0.0849, wR2 = 0.2398
Largest diff. peak/hole / e Å^{-3}	1.49/-1.50

Table S3. Crystal data and structure refinement for CPM-70-Ni

Empirical formula	$C_{57}H_{33}N_3Ni_3O_{13}$
Formula weight	1143.99
Temperature/K	296.15
Crystal system	trigonal
Space group	*R*-3*c*
a /Å	19.1393(7)
b /Å	19.1393(7)
c /Å	45.836(3)
α /°	90
β /°	90
γ /°	120
Volume/Å^3	14541.0(15)
Z	6
ρcalcg/cm^3	0.784
μ/mm^{-1}	0.986
F(000)	3504.0
Radiation	CuKα (λ = 1.54178)
2θ range for data collection/°	6.58 to 130.14
Index ranges	-22 ≤ h ≤ 22, -22 ≤ k ≤ 17, -47 ≤ l ≤ 53
Reflections collected	46965
Independent reflections	2766 [Rint = 0.0321, Rsigma = 0.0164]
Data/restraints/parameters	2766/18/117
Goodness-of-fit on F^2	1.050
Final R indexes [I>=2σ (I)]	R1 = 0.0466, wR2 = 0.1302
Final R indexes [all data]	R1 = 0.0491, wR2 = 0.1338
Largest diff. peak/hole / e Å^{-3}	0.55/-0.45

Section S3 Characterization of MOFs

Stability analysis of MOFs

Scanning electron microscopy (SEM) of MOFs

SEM was used to examine the morphology of MOFs series. The SEM images of these MOFs were collected on a Merlin Compact FEI Verios-460. Samples were prepared by sprinkling directly onto the sample stages. Furthermore, the elements inside the MOF were demonstrated by the energy dispersive spectroscopy (EDS) of MOF samples.

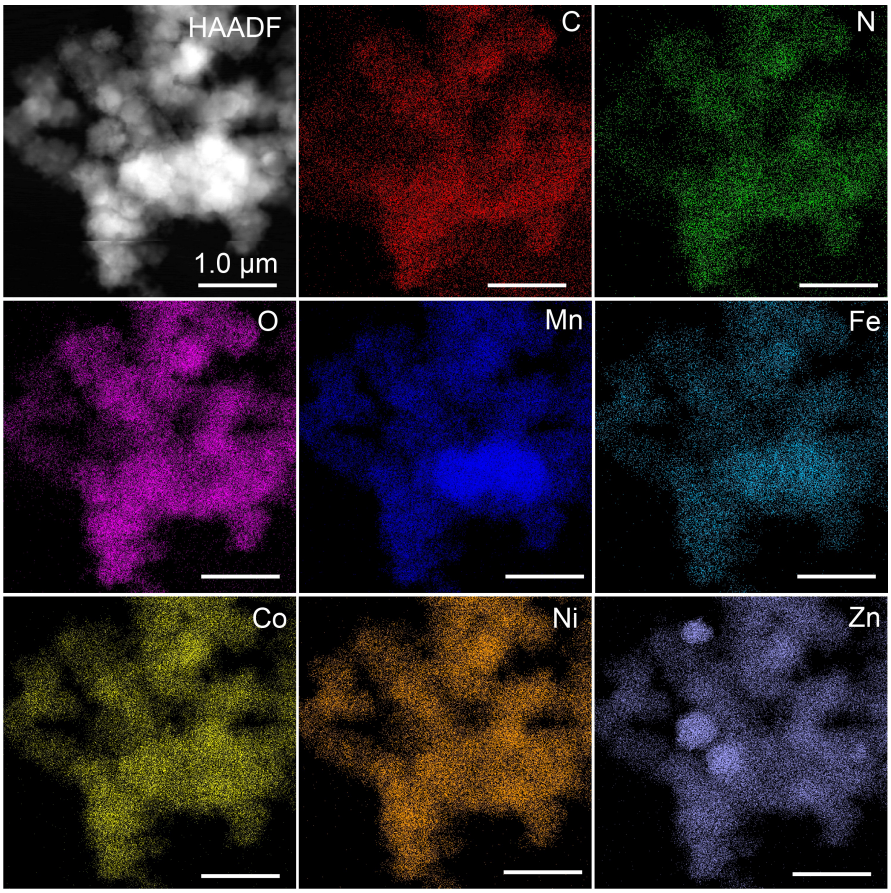

Fig. S17 The elemental mappings of the CPM-70-MnFeCoNiZn by TEM.

N_2 adsorptions analysis of MOFs

The porosity of CPM-70 MOF series was assessed by N_2 adsorption analysis. N_2 isotherms were measured on a Quantachrome Autosorb iQ_2 automatic volumetric instrument. The temperature of N_2 isotherms at 77 K was controlled using a liquid nitrogen bath. To estimate pore size distribution for these MOF samples, non-local density

functional theory (NLDFT) (S3) based on a carbon model was used for the fitting of N_2 isotherms at 77 K, ranging from 920 to 1930 m^2/g (Fig. S18 to S25).

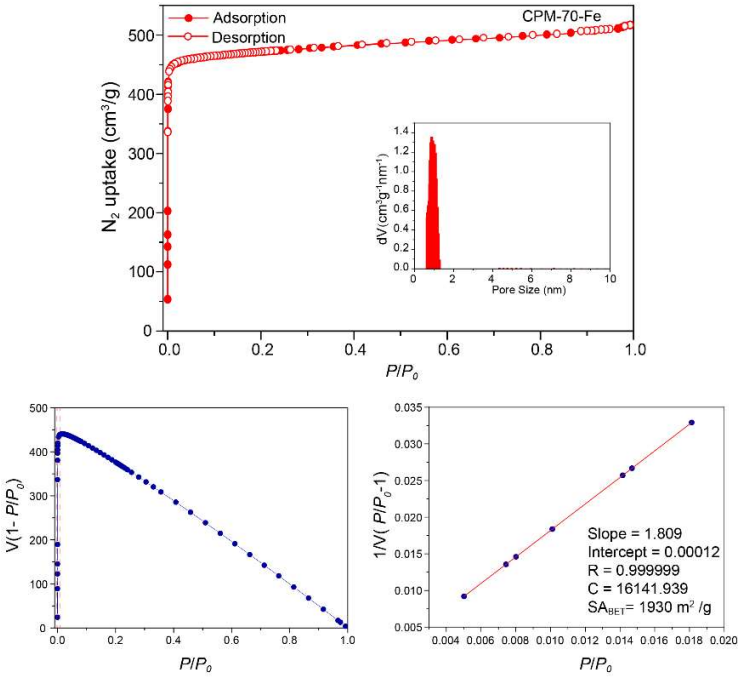

Fig. S18 N_2 isotherm of CPM-70-Fe at 77 K. Open and filled symbols represent adsorption and desorption balance, respectively. Insert, pore distribution of CPM-70-Fe.

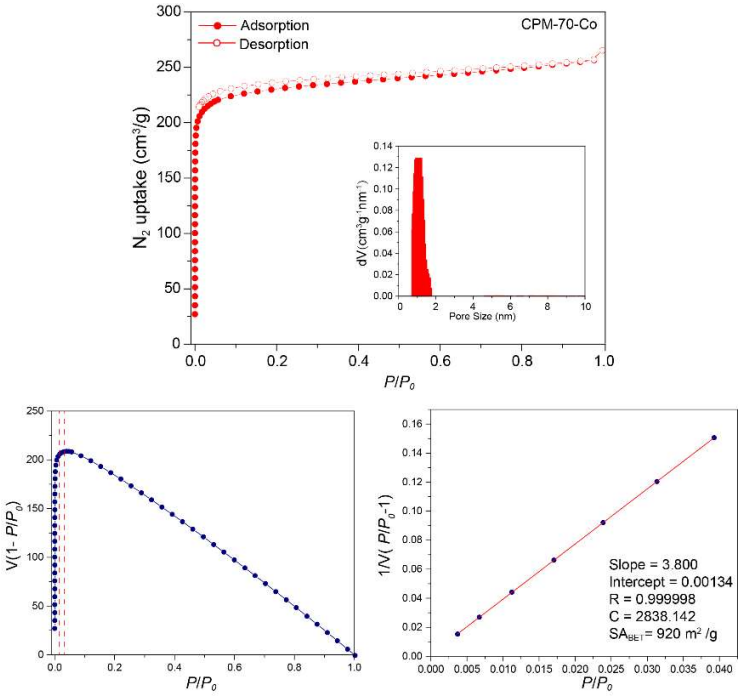

Fig. S19 N_2 isotherm of CPM-70-Co at 77 K. Open and filled symbols represent adsorption and

desorption balance, respectively. Insert, pore distribution of CPM-70-Co.

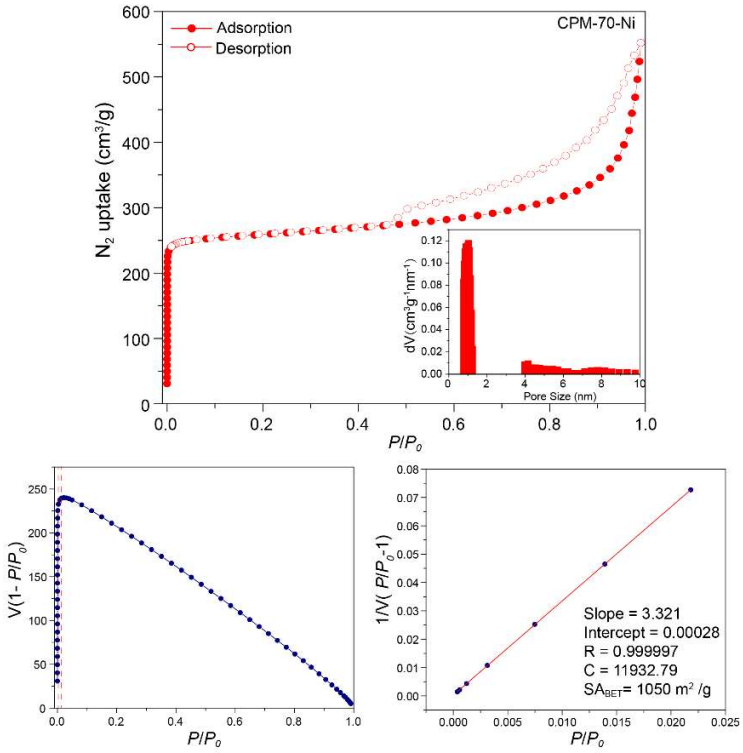

Fig. S20 N_2 isotherm of CPM-70-Ni at 77 K. Open and filled symbols represent adsorption and desorption balance, respectively. Insert, pore distribution of CPM-70-Ni.

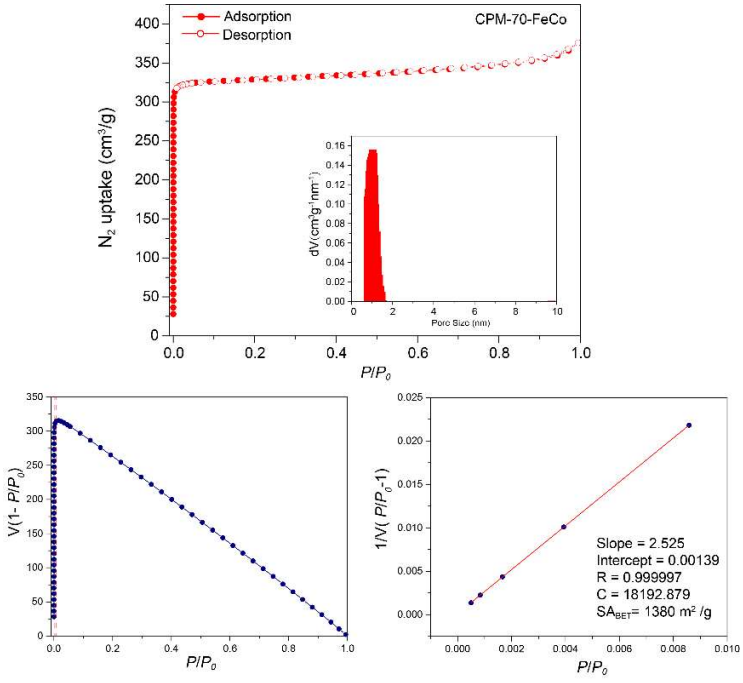

Fig. S21 N_2 adsorption isotherm of CPM-70-FeCo at 77 K. Open and filled symbols represent

adsorption and desorption balance, respectively. Insert, pore distribution of CPM-70-FeCo.

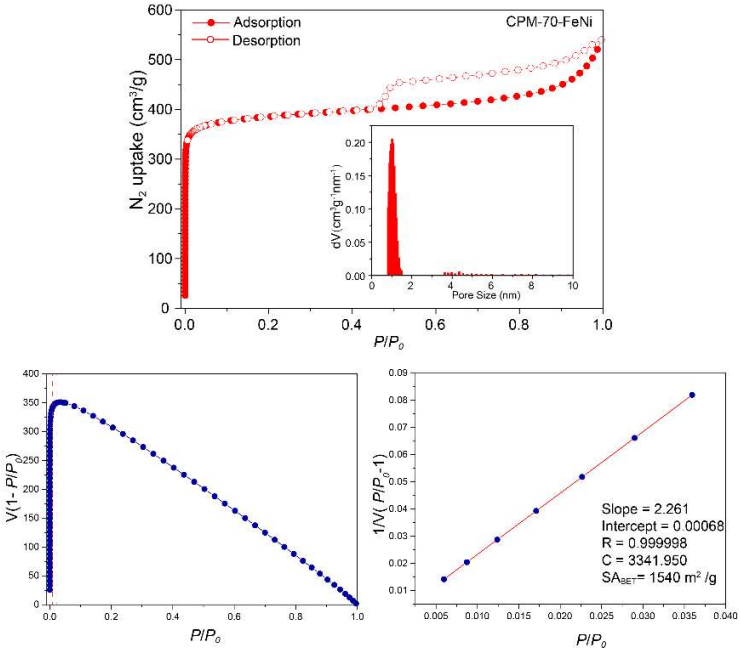

Fig. S22 N_2 adsorption isotherm of CPM-70-FeNi at 77 K. Open and filled symbols represent adsorption and desorption balance, respectively. Insert, pore distribution of CPM-70-FeNi.

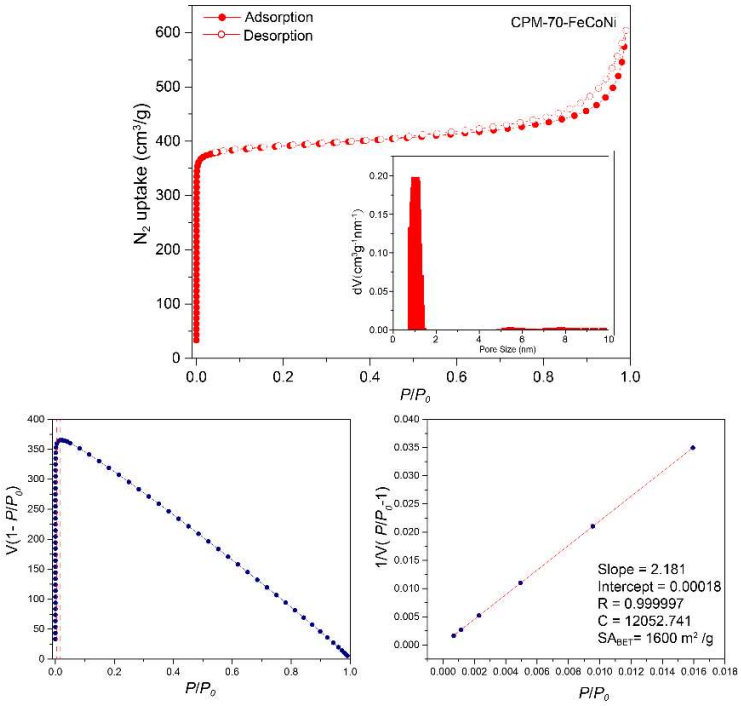

Fig. S23 N_2 adsorption isotherm of CPM-70-FeCoNi at 77 K. Open and filled symbols represent adsorption and desorption balance, respectively. Insert, pore distribution of CPM-70-FeCoNi.

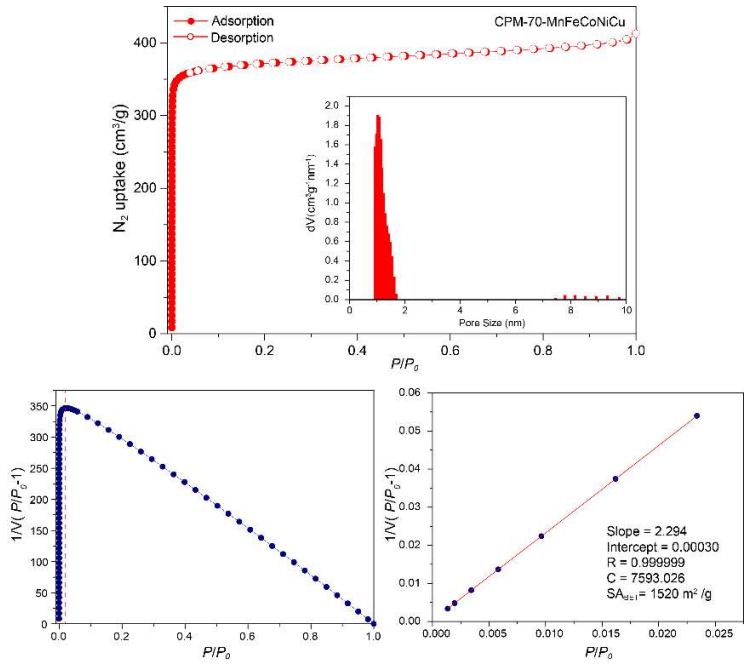

Fig. S24 N_2 adsorption isotherm of CPM-70-MnFeCoNiCu at 77 K. Open and filled symbols represent adsorption and desorption balance, respectively. Insert, pore distribution of CPM-70-MnFeCoNiCu.

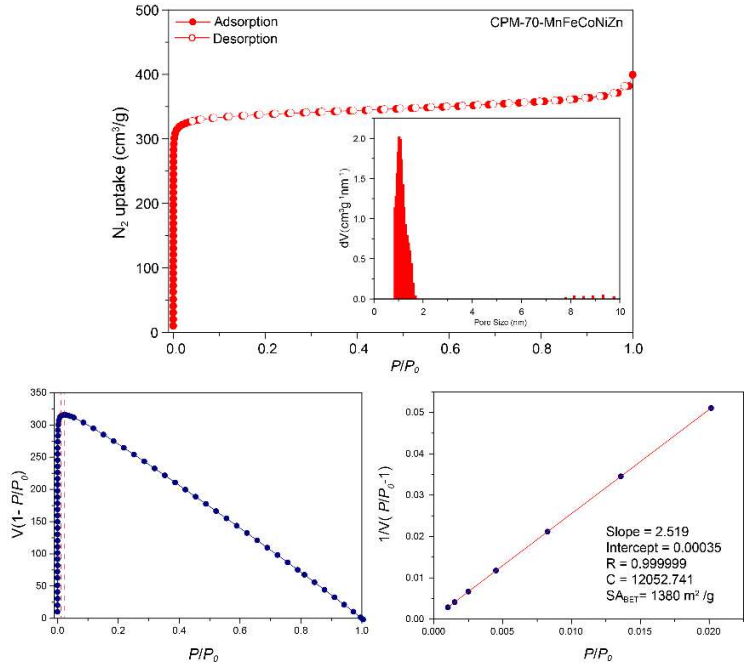

Fig. S25 N_2 adsorption isotherm of CPM-70-MnFeCoNiZn at 77 K. Open and filled symbols represent adsorption and desorption balance, respectively. Insert, pore distribution of CPM-70-MnFeCoNiZn.

METHODS:

The activated MOF samples were immersed in aqueous solutions with different pH values for 6 h at room temperature. After that, these samples were immersed in acetone for three times at room temperature. The crystallinity of these MOFs was confirmed by powder X-ray diffraction (PXRD) technique.

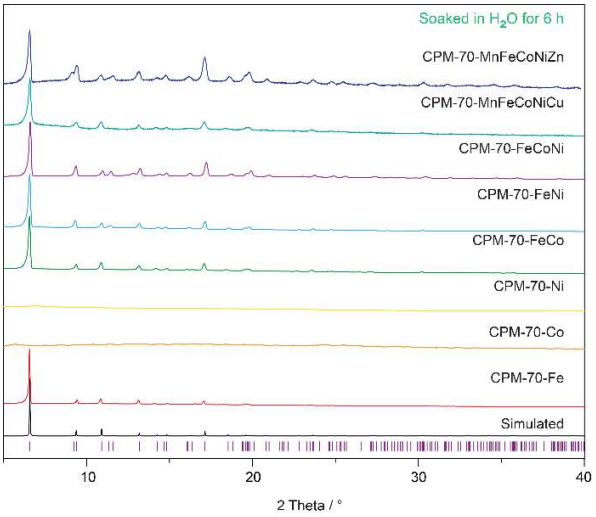

Fig. S26 MOFs in H_2O for 6 h.

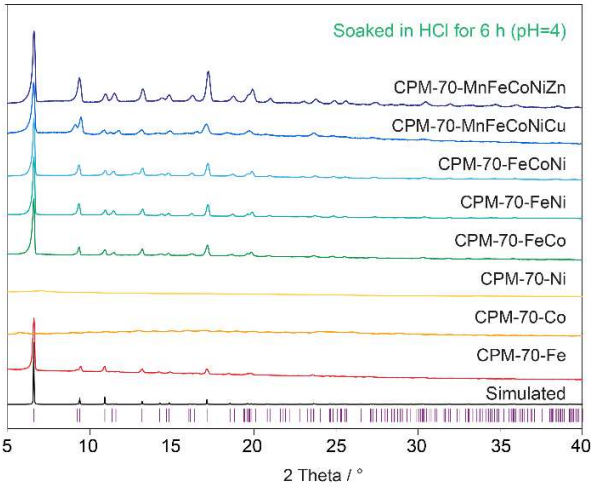

Fig. S27 MOFs in HCl (pH=4) for 6 h.

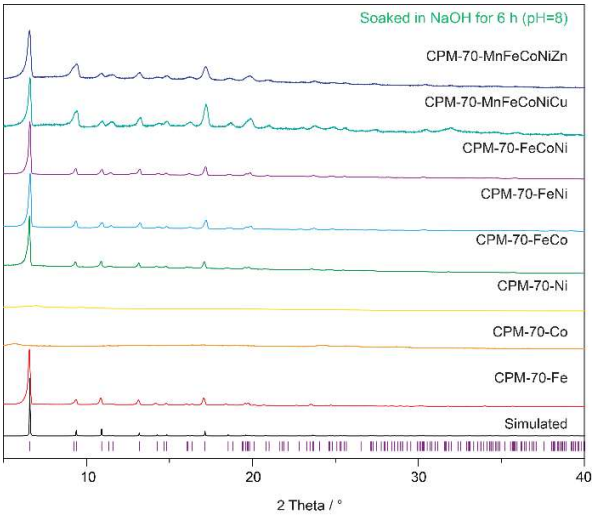

Fig. S28 MOFs in NaOH (pH = 8) for 6 h.

Thermogravimetric analysis of MOFs

METHODS:

Activated MOFs were put in different All TG analyses were performed on a TA Instruments NETZSCH STA449 C series thermal gravimetric analyzer with samples held in aluminum oxide pans in a continuous air flow atmosphere. The heating rate was set to 10 °C/min from room temperature to 800 °C for all TGA experiments.

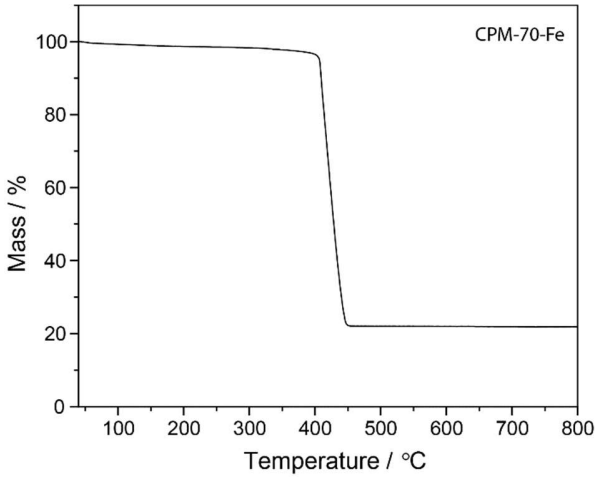

Fig. S29 TGA plot of activated CPM-70-Fe

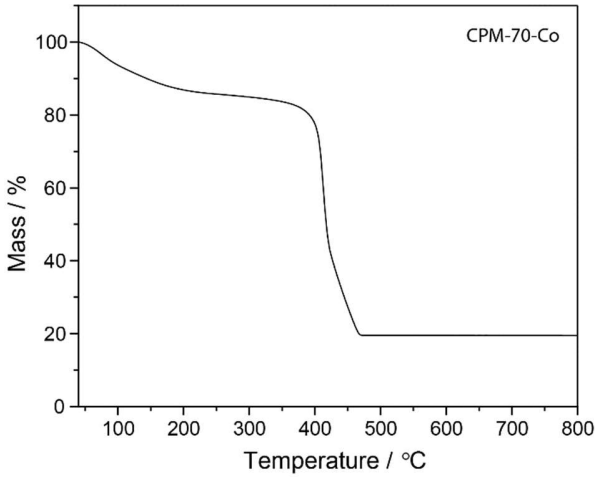

Fig. S30 TGA plot of activated CPM-70-Co

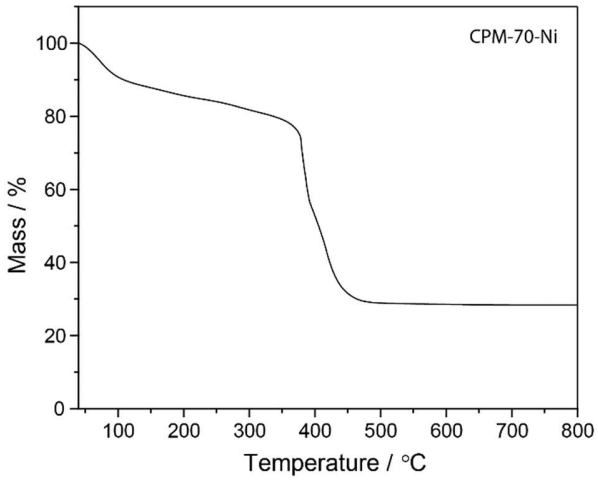

Fig. S31 TGA plot of activated CPM-70-Ni

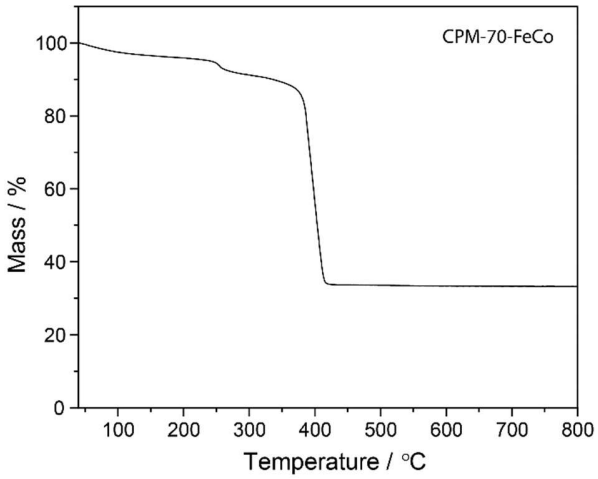

Fig. S32 TGA plot of activated CPM-70-FeCo

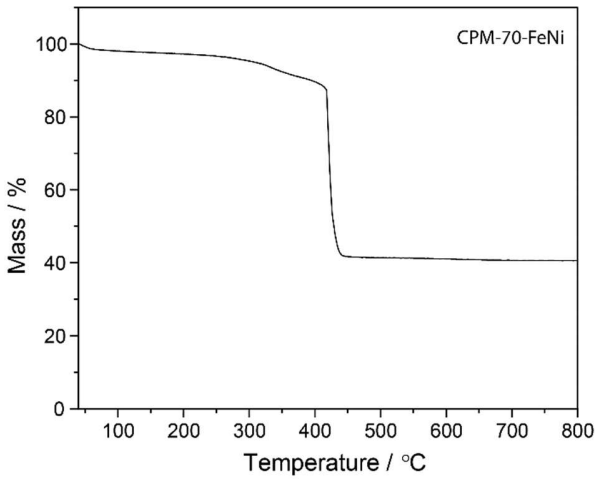

Fig. S33 TGA plot of activated CPM-70-FeNi

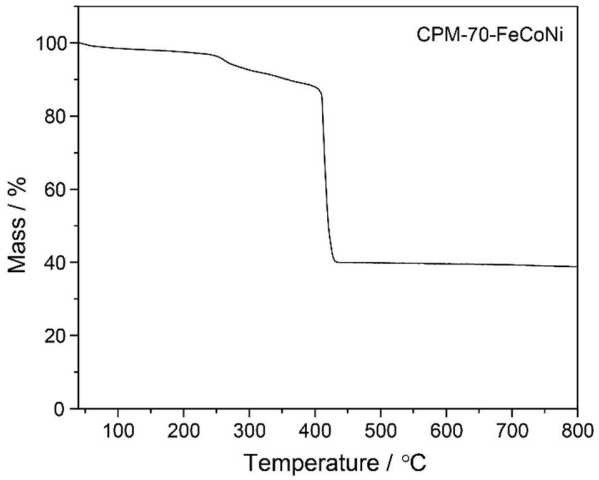

Fig. S34 TGA plot of activated CPM-70-FeCoNi

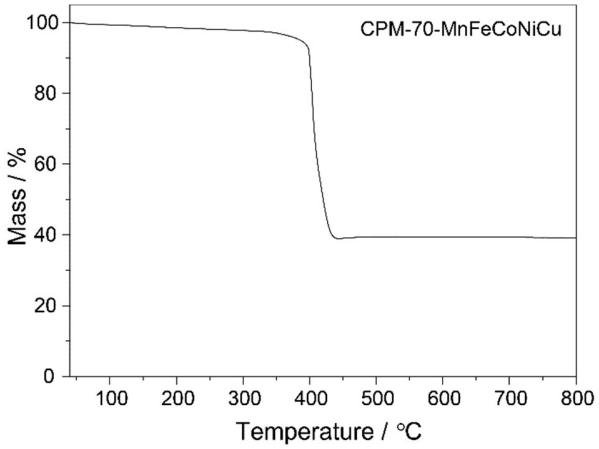

Fig. S35 TGA plot of activated CPM-70-MnFeCoNiCu

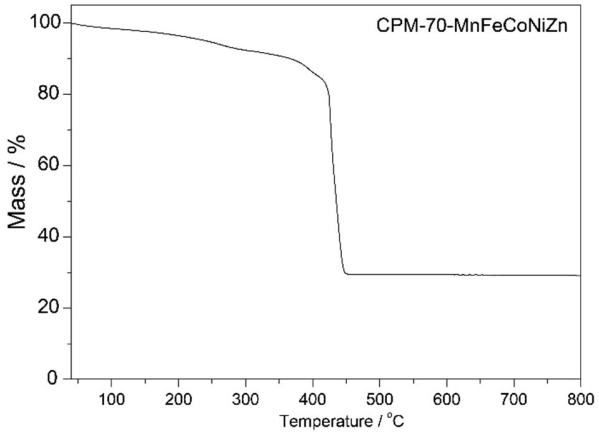

Fig. S36 TGA plot of activated CPM-70-MnFeCoNiZn

ICP results of MOFs

ICP-AES analysis was used to precisely determine the real metal ions ratio in our MOF samples. All ICP-AES experiments were performed on a plasma-optical emission spectrometer of Leeman Labs Prodigy 7. Aqua regia was used to digest the activated MOFs.

Table S4 ICP results of MTV-MOFs

Compound	Feed ratio (mole)	Actual ratio (mg/L)	Actual ratio (mole)
CPM-70-FeCo	1:1	28.7 : 46.4	1 : 1.53
CPM-70-FeNi	1:1	35.1 : 91.2	1 : 2.47
CPM-70-FeCoNi	1:1:1	25.5 : 32.9 : 34.8	1 : 1.22 : 1.30
CPM-70-MnFeCoNiCu	1:1:1:1:1	27.1:40.2:40.1:34.9:31.8	1 : 1.41 : 1.41 : 1.31 : 1.03
CPM-70-MnFeCoNiZn	1:1:1:1:1	23.5:32.7:37.9:35.9:41.0	1 : 1.32 : 1.54 : 1.55 : 1.49

Section S4 Synthesis and characterization of MOF-laser

Synthesis of MOF-laser

Activated MOF samples (16 mg) was loaded in a hole (19 mm) of a copper foil with thickness of 10 μm and then sandwiched by two glass slides and fixed with scotch tape. The laser system was mainly consisted of a nanosecond pulse fiber laser (YLP-0.5-80-20-10, IPG photonics) for energy source, a galvanometer (6240H, Cambridge Technology Inc.) for beam scanning and a focus lens (FTheta-Ronar, LINOS) for beam concentration. The laser parameter was easily adjusted by software embedded in a computer. In a typical laser scribing, the sample was placed on a XYZ stage (Suruga Seiki) and the focus length was

adjusted to 350 mm. The pulse laser with wavelength of 1064 nm and pulse duration of 80 ns was adjusted at frequency of 20 kHz with the laser beam spot size of 200 μm. The laser power was set at the range of 3.5 to 7.5 w and carefully measured by an optic power meter (OPHIR). The laser scanning route was set at a line-by-line model with a line distance of 80 μm and speed of 75 mm s^{-1}. The MOF-laser used for oxygen evaluation reaction (OER) was obtained at laser power of 4.5 w at scanning speed of 75 mm s^{-1}.

Scanning electron microscopy (SEM) of MOF-laser

SEM was used to examine the morphology of MOFs series (Fig. S37 to S44). Samples were directly dispersed in absolute acetone and then dropped on a silicon wafer for further morphology observation by using SEM, which was carried out on an FEI Verios 460 Schottky type field emission SEM with through-lens-detector under an ultralow accelerating voltage of 500 V. EDX spectroscopy for element mapping was carried out using an Oxford Ultim Extreme large-area silicon drift detector detector to confirm the homogeneous distribution of metals in as-prepared MOFs.

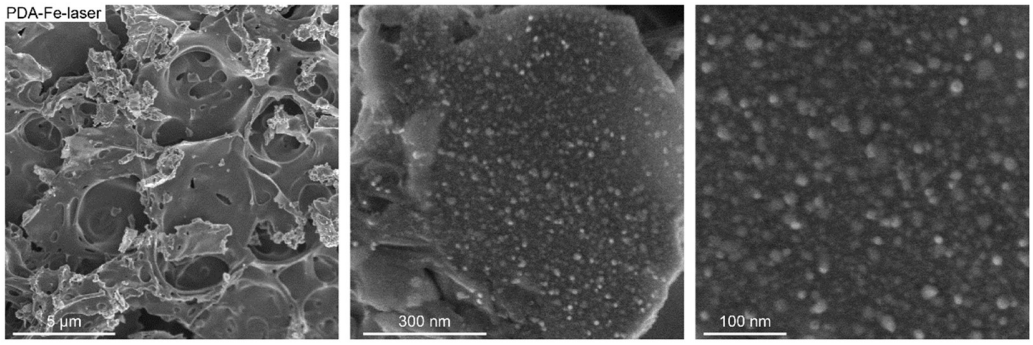

Fig. S37 SEM images of CPM-70-Fe-laser.

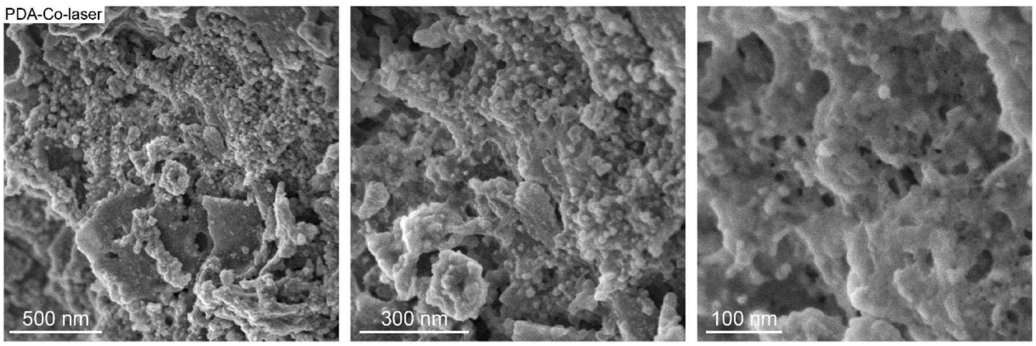

Fig. S38 SEM images of CPM-70-Co-laser.

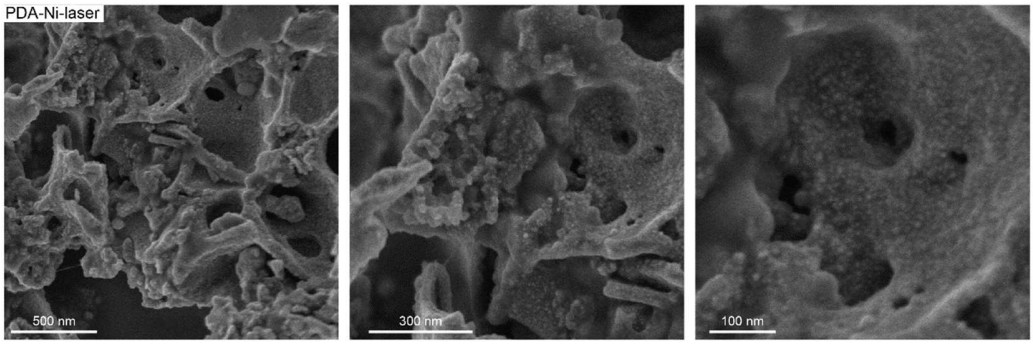

Fig. S39 SEM images of CPM-70-Ni-laser.

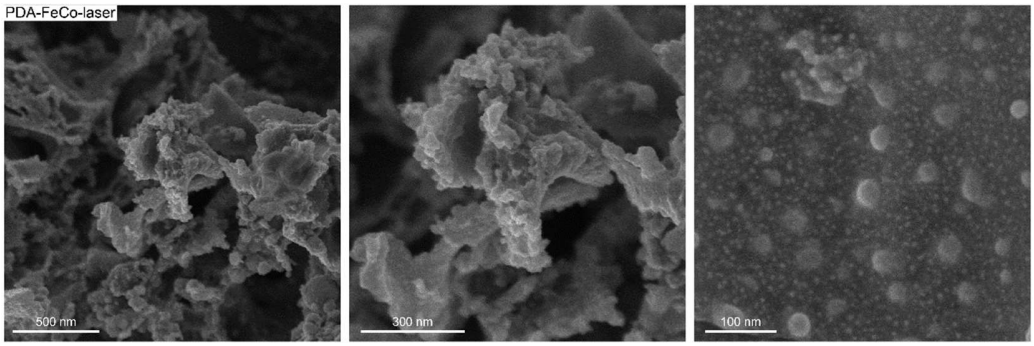

Fig. S40 SEM images of CPM-70-FeCo-laser.

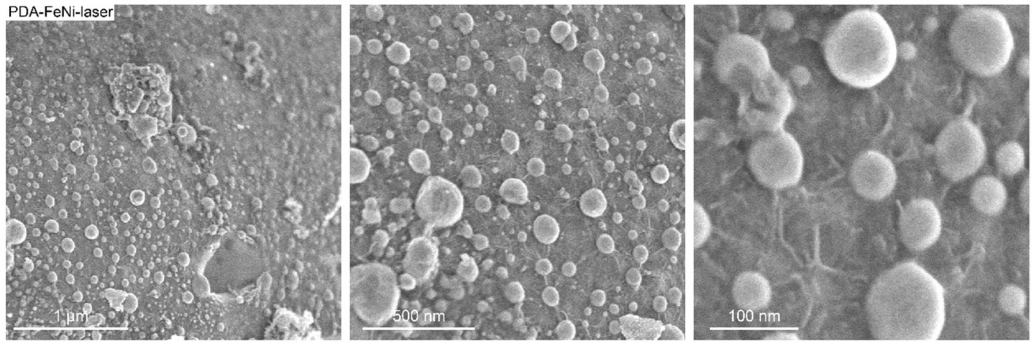

Fig. S41 SEM images of CPM-70-FeNi-laser.

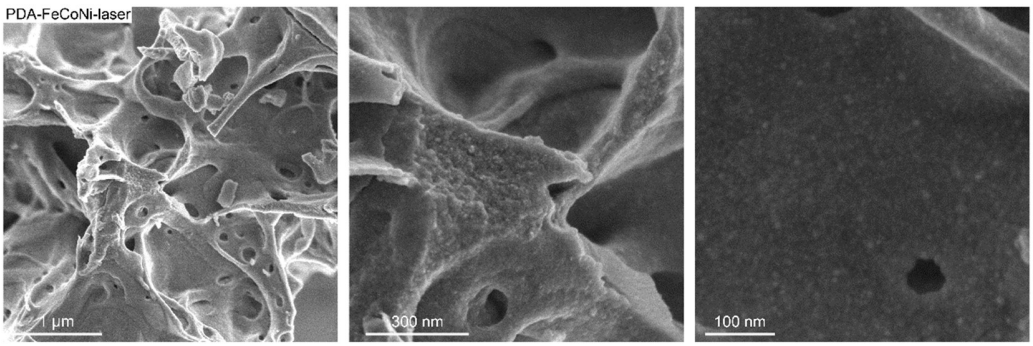

Fig. S42 SEM images of CPM-70-FeCoNi-laser.

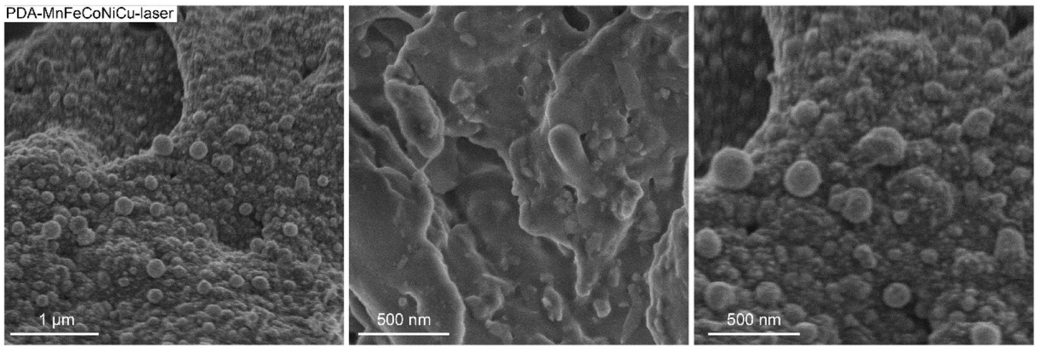

Fig. S43 SEM images of CPM-70-MnFeCoNiCu-laser.

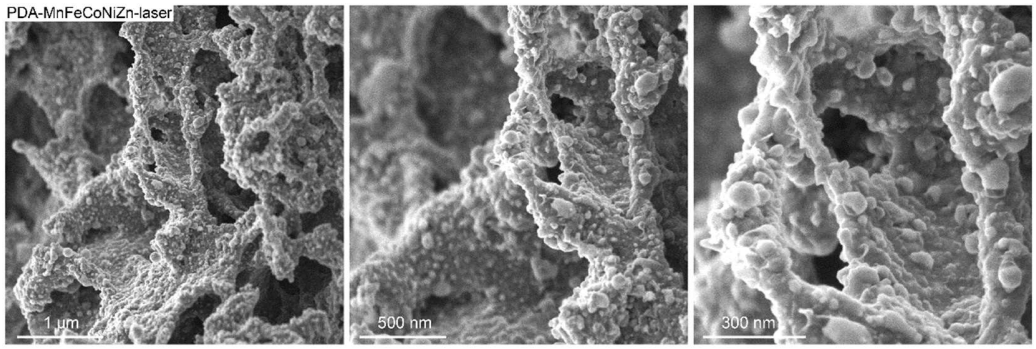

Fig. S44 SEM images of CPM-70-MnFeCoNiZn-laser.

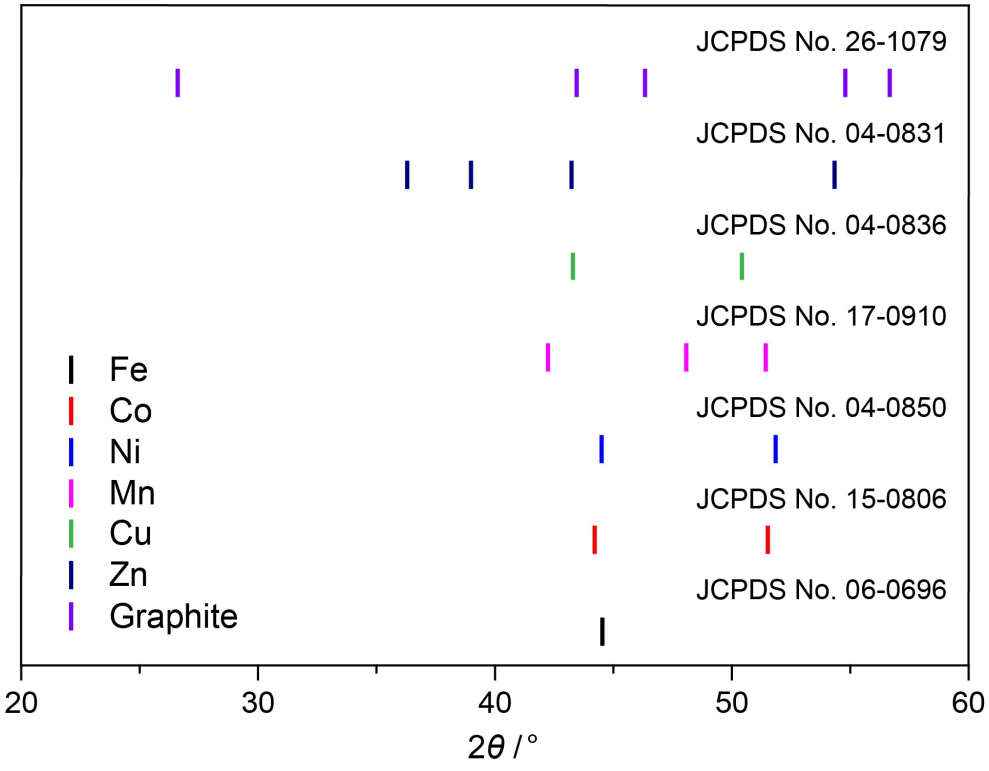

Fig. S45 The PXRD patterns of single-component metal nanoparticles from JCPDS

Transmission Electron Microscopes (TEM) of MOF-laser

A JEOL JEM-2100 Plus Schottky-type field emission transmission electron microscope equipped with a Gatan Oneview CMOS 4k detector was operated at 200 kV to obtain transmission electron micrographs. The samples were first dispersed in absolute ethanol with ultrasonic treatment, and then transferred onto a carbon-coated molybdenum grid and dried in air.

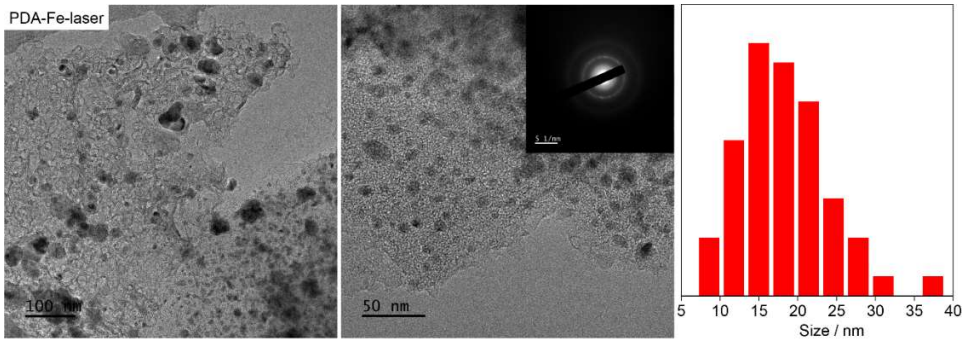

Fig. S46 TEM images, diffraction patterns and particle size distribution plot of CPM-70-Fe-laser

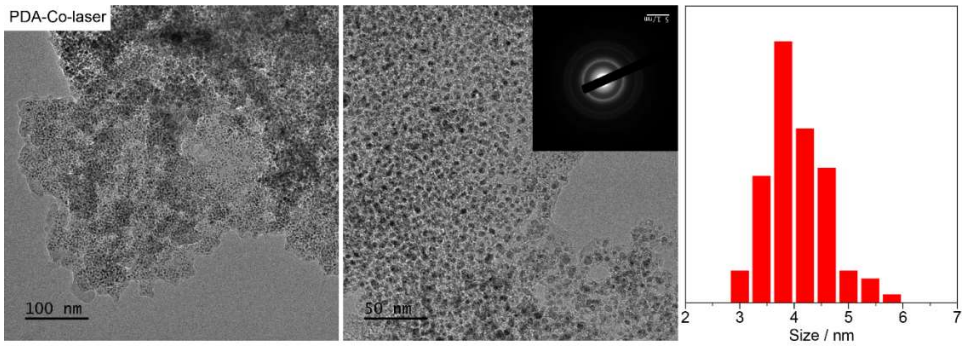

Fig. S47 TEM images, diffraction patterns and particle size distribution plot of CPM-70-Co-laser

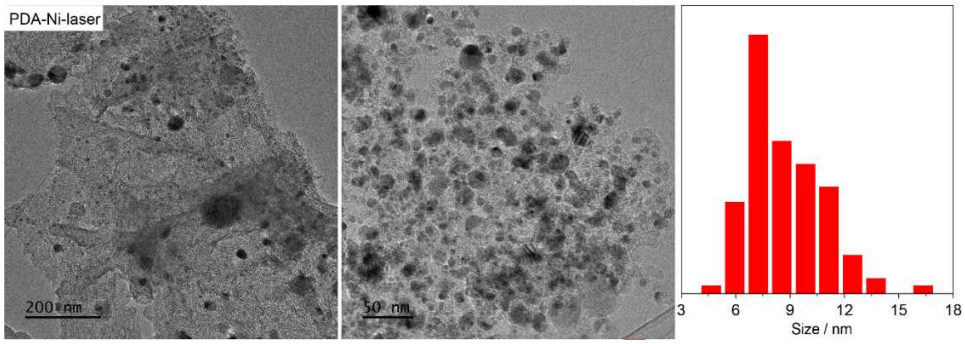

Fig. S48 TEM images, diffraction patterns and particle size distribution plot of CPM-70-Ni-laser

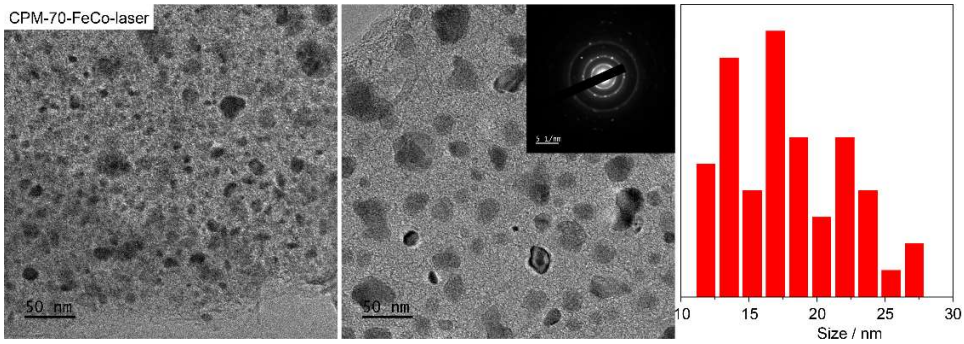

Fig. S49 TEM images, diffraction patterns and particle size distribution plot of CPM-70-FeCo-laser

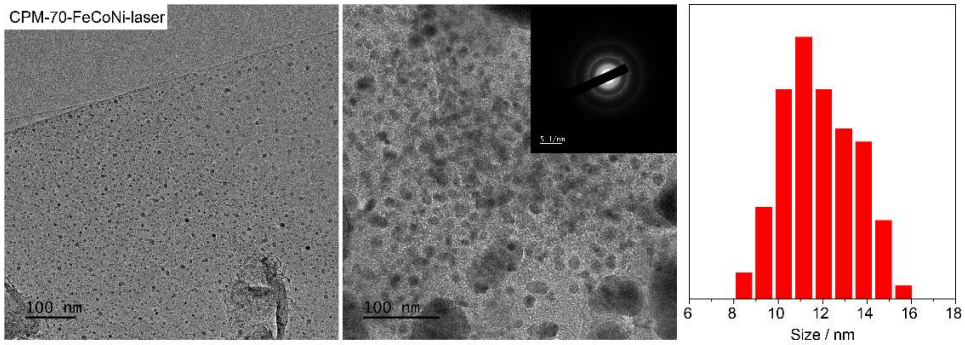

Fig. S50 TEM images, diffraction patterns and particle size distribution plot of CPM-70-FeCoNi-laser

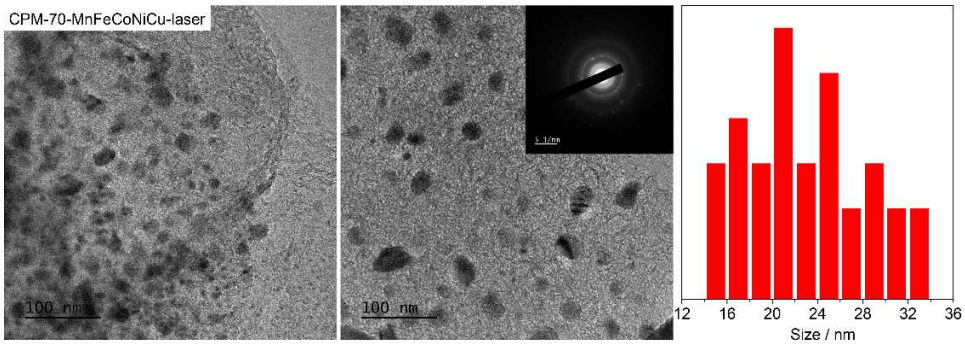

Fig. S51 TEM images, diffraction patterns and particle size distribution plot of CPM-70-MnFeCoNiCu-laser

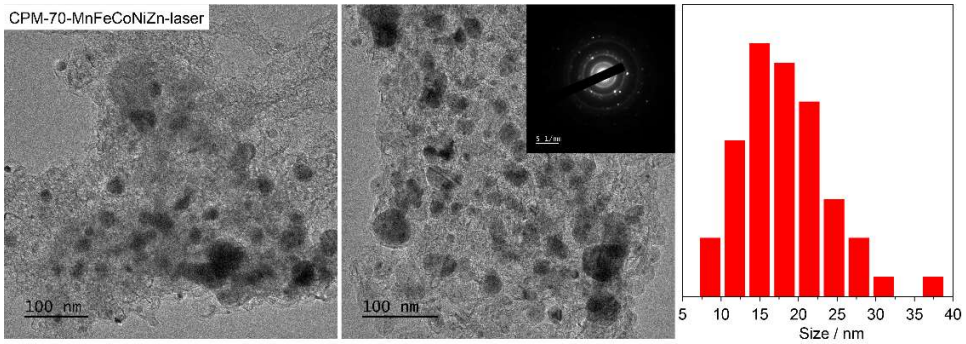

Fig. S52 TEM images, diffraction patterns and particle size distribution plot of CPM-70-MnFeCoNiZn-laser

ICP-AES results of MOF-laser

ICP-AES analysis was used to precisely determine the real metal ions ratio in our MOF-laser samples. All ICP-AES experiments were performed on a plasma-optical emission spectrometer of Leeman Labs Prodigy 7. Aqua regia was used to digest the activated MOFs.

Table S5. ICP results of MOF-laser

Compound	Feed ratio (mole)	Actual ratio (mg/L)	Actual ratio (mole)
CPM-70-FeCo-laser	1:1	2.92 : 5.95	1 : 1.93
CPM-70-FeNi-laser	1:1	2.30 : 7.27	1 : 3.01
CPM-70-FeCoNi-laser	1:1:1	2.74 : 3.98 : 4.01	1 : 1.38 : 1.39
CPM-70-MnFeCoNiCu-laser	1:1:1:1:1	2.44:4.98:4.73:4.20:5.43	1: 1.93 : 1.84 : 1.75 : 1.95
CPM-70-MnFeCoNiZn-laser	1:1:1:1:1	2.42:3.43:3.20:3.36:4.2	1 : 1.34 : 1.26 : 1.41 : 1.48

XPS analysis of MOF-laser

XPS was performed on a Thermo Fisher ESCALAB 250Xi using a monochromatic Al Ka X-ray source. All the binding energies were referenced to the C 1s peak (284.8 eV) arising from adventitious carbon. The energy scales were aligned by using the Fermi level of the XPS instrument (4.57 eV versus absolute vacuum value).

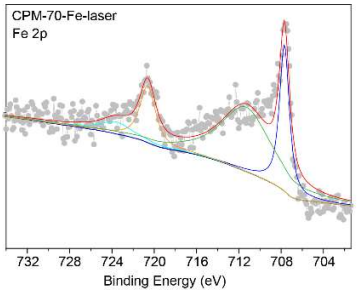
CPM-70-Fe-laser
Fe 2p
732 728 724 720 716 712 708 704
Binding Energy (eV)

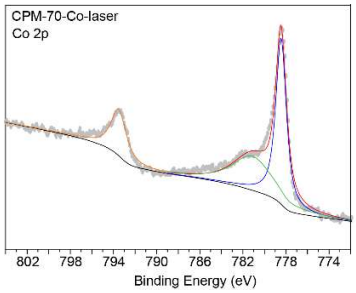
CPM-70-Co-laser
Co 2p
802 798 794 790 786 782 778 774
Binding Energy (eV)

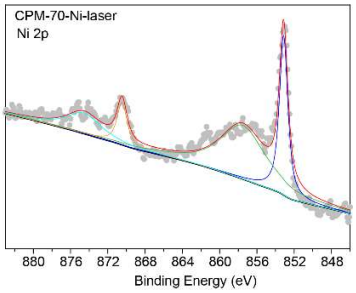
CPM-70-Ni-laser
Ni 2p
880 876 872 868 864 860 856 852 848
Binding Energy (eV)

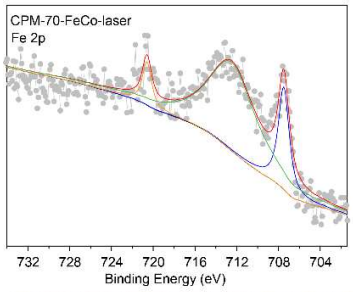
CPM-70-FeCo-laser
Fe 2p
732 728 724 720 716 712 708 704
Binding Energy (eV)

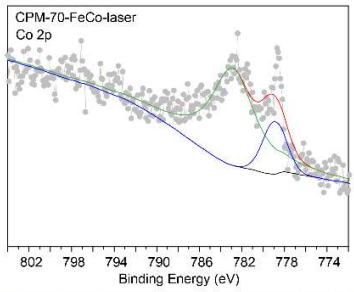
CPM-70-FeCo-laser
Co 2p
802 798 794 790 786 782 778 774
Binding Energy (eV)

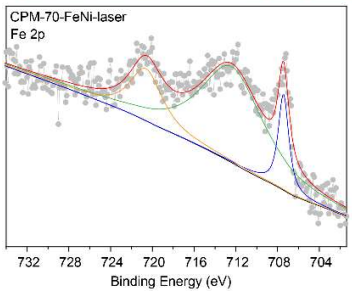
CPM-70-FeNi-laser
Fe 2p
732 728 724 720 716 712 708 704
Binding Energy (eV)

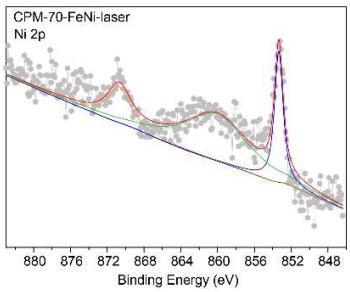
CPM-70-FeNi-laser
Ni 2p
880 876 872 868 864 860 856 852 848
Binding Energy (eV)

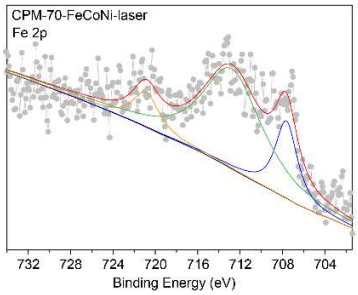
CPM-70-FeCoNi-laser
Fe 2p
732 728 724 720 716 712 708 704
Binding Energy (eV)

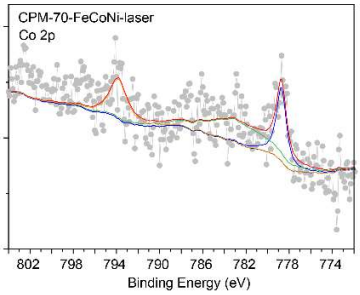
CPM-70-FeCoNi-laser
Co 2p
802 798 794 790 786 782 778 774
Binding Energy (eV)

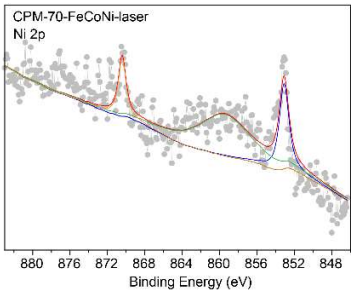
CPM-70-FeCoNi-laser
Ni 2p
880 876 872 868 864 860 856 852 848
Binding Energy (eV)

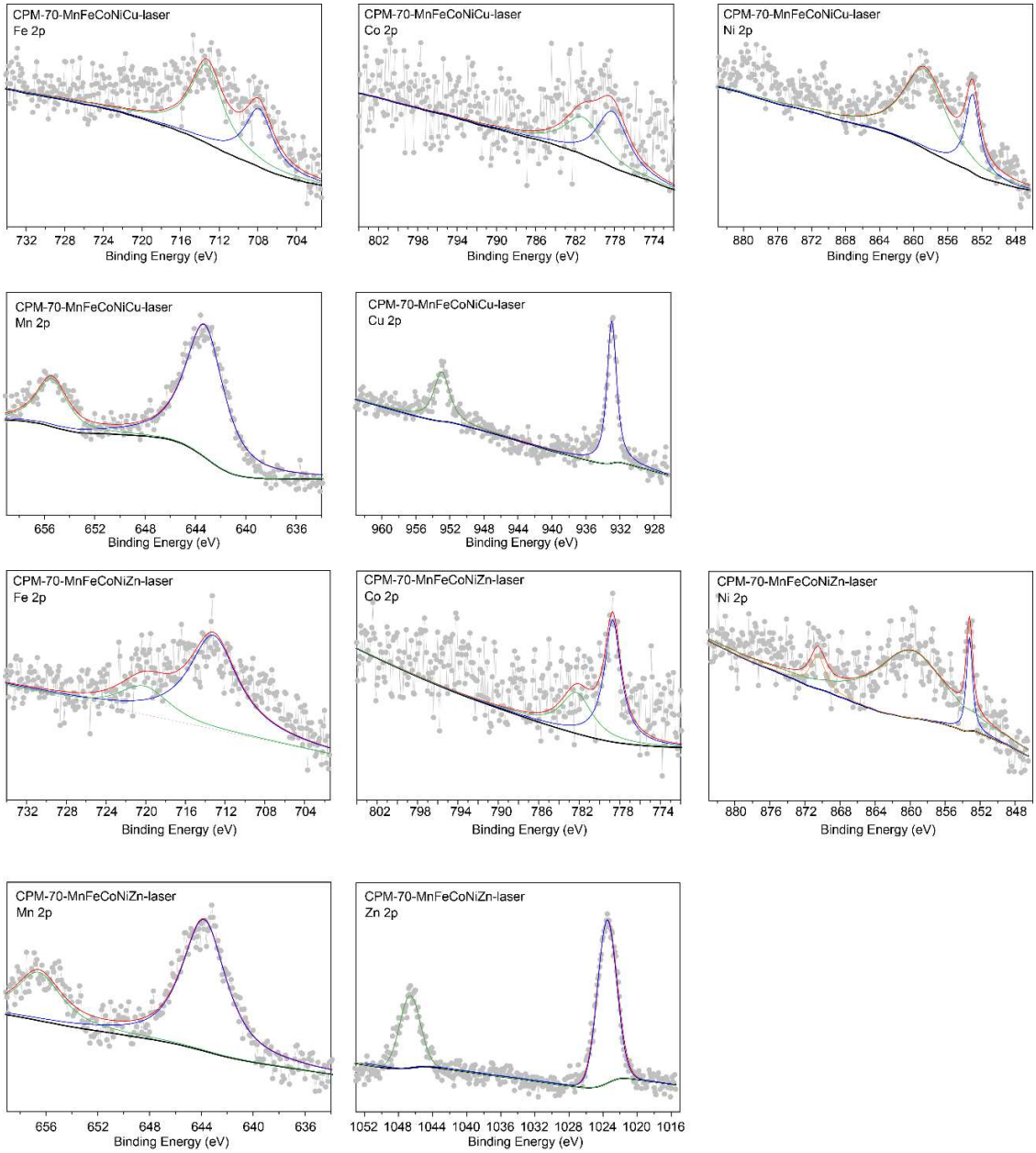

Fig. S53 XPS analysis of MOF-laser

Raman spectrum of MOF-laser

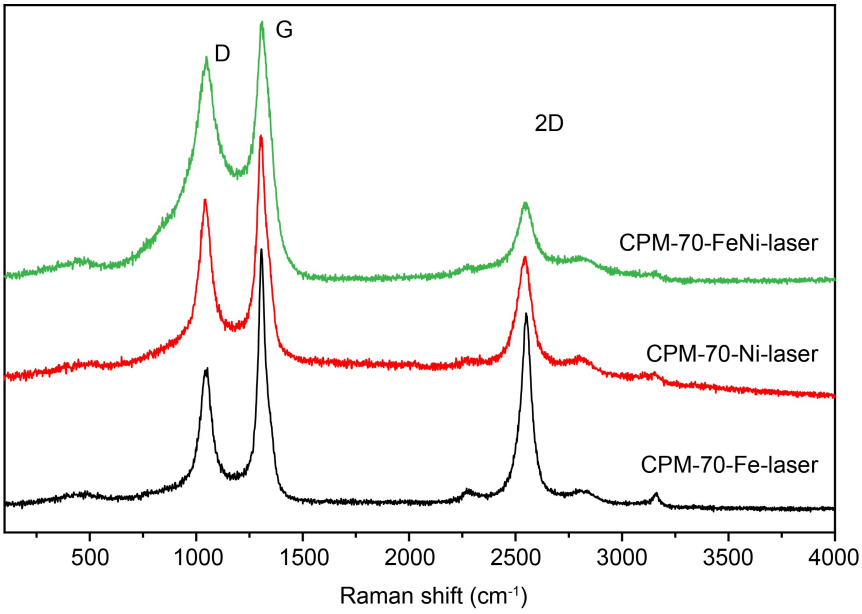

Fig. S54 Raman spectrum of MOF-laser

References

S1. Kolychev E. L., Asachenko A. F., Dzhevakov P. B., Bush A. A., Shuntikov V. V., Khrustalev V. N., Nechaev M. S. Dalton Trans. 42 (2013) 6859-6866.

S2. Zhang L. Y., Zhang Y. X., Dong J. Z., Liu J., Zhang L. Y., Sun H. B. Bioorg. Med. Chem. Lett. 22 (2012) 1036-1039.

S3. Walton, K S.; Snurr, R Q. J. Am. Chem. Soc. 129 (2007) 8552-8556.